Ultrahigh-Speed Traveling-Wave Electroabsorption Modulator—Design and Analysis

G. L. Li, *Student Member, IEEE,* C. K. Sun, S. A. Pappert, W. X. Chen, and P. K. L. Yu, *Senior Member, IEEE*

***Abstract*—Theoretical analysis and numerical calculations are presented for ultrahigh-speed (>50 GHz) traveling-wave electroabsorption modulators (TW-EAM's), including effects of velocity mismatch, impedance mismatch, and microwave attenuation. A quasi-static equivalent circuit model is used to examine the TW-EAM microwave properties, including the effect of photocurrent. Due to the optical propagation loss of the waveguide, the TW-EAM waveguide length for maximum RF link gain is currently limited to 200–300 μm. The discussion indicates that the carrier transit time in the intrinsic layer may not severely limit the TW-EAM bandwidth. Three TW-EAM design approaches are discussed: low-impedance matching; reducing the waveguide capacitance; and distributing the modulation region.**

***Index Terms*— Analog fiber links, electroabsorption modulators, traveling wave.**

I. Introduction

HIGH-SPEED electroabsorption modulators (EAM's) are getting more and more interest for use in both digital and analog high-speed fiber-optic links. A 50-GHz bandwidth lumped EAM (L-EAM) has been reported with the active waveguide length shortened to 63 μm [1]. However, reducing the waveguide length results in smaller modulation efficiency due to both shorter modulation length and smaller power handling ability. To overcome the resistance–capacitance (*RC*) bandwidth limit without severely sacrificing modulation efficiency, the traveling-wave EAM (TW-EAM) has been proposed and experimentally investigated by several authors [2]–[4]. A 50-GHz optical bandwidth (~30-GHz electrical bandwidth) has been reported for a 200-μm-long TW-EAM [2].

In a TW-EAM, the electrode is designed as a transmission line to distribute the capacitance over the entire device length. This allows a longer modulation length to enhance the modulation efficiency while maintaining a large bandwidth. To achieve an optimum modulator performance, the microwave phase velocity should match with the optical group velocity [5], [6] in the TW-EAM waveguide; perfect microwave impedance matching and optical antireflection coating are desired; and microwave attenuation as well as optical propagation loss should be eliminated. For a typical EAM waveguide, as discussed later, it is very difficult to achieve good impedance matching and velocity matching, and optical and microwave attenuation losses are fairly large. This compounds the difficulty in designing an ultrahigh-speed TW-EAM with high modulation efficiency.

However, practical approaches still exist for producing a TW-EAM with electrical bandwidth $>$ 50 GHz and performance better than that of an L-EAM device. TW-EAM frequency response is derived in Section II to provide a design guideline. In Section III, the optimal modulator length for maximizing RF gain is analyzed. In Section IV, a quasi-static equivalent circuit model is employed to estimate the frequency dependent microwave properties of a standard EAM waveguide, including the effect of photocurrent. In Section V, effects of carrier transit time on the bandwidth of TW-EAM's are discussed. In Section VI, three approaches for achieving the ultrahigh-speed TW-EAM are discussed: low-impedance matching; reducing the waveguide capacitance; and distributing the modulation region.

II. Modulator Frequency Response

The optical power output from an EAM can be expressed as

$$I_{\text{out}} = I_{\text{in}} C^2 \exp(-\alpha_o L) \exp\left\{-\gamma \int_0^L \alpha(x)\, dx\right\} \quad (1)$$

where I_{in} is the input optical power, C is the optical loss factor at each facet, α_o is the optical attenuation coefficient inside the modulator at zero bias voltage, γ is the optical confinement factor in the modulator absorption layer, and $\alpha(x)$ denotes the absorption change due to the nonzero voltage applied across the absorption layer. The absorption change $\alpha(x)$ consists of a dc part α_b at the bias voltage V_b, and an ac part due to the modulation voltage V_{ac} which can be approximated as $(d\alpha_b/dV_b)V_{\text{ac}}(x)$. Using a small-signal approximation, we obtain the ac part in (1)

$$I_{\text{ac}} = -I_{\text{in}} C^2 \exp(-\alpha_o L - \gamma \alpha_b L)\gamma \frac{d\alpha_b}{dV_b} \int_0^L V_{\text{ac}}(x)\, dx. \quad (2)$$

All terms except V_{ac} are independent of microwave frequency. The microwave power received by the photodetector is proportional to $|I_{\text{ac}}|^2$, so that the radio-frequency (RF) link gain is proportional to $|\int_0^L V_{\text{ac}}(x)\, dx|^2$. Including multiple microwave reflections inside the modulator [7], V_{ac} can be

Manuscript received October 12, 1998; revised March 10, 1999. This work was supported in part by Defense Advanced Research Projects Agency and in part by the Office of Naval Research.

G. L. Li, W. X. Chen, and P. K. L. Yu are with the Department of Electrical and Computer Engineering, University of California at San Diego, La Jolla, CA 92093-0407 USA.

C. K. Sun and S. A. Pappert are with SPAWAR Systems Center, San Diego, CA 92152-5001 USA.

Publisher Item Identifier S 0018-9480(99)05187-X.

expressed as

$$V_{\rm ac}(x,t) = \frac{V_0 T \exp(j\omega t)}{1-\Gamma_L\Gamma_S \exp(-2\gamma_\mu L)} \cdot \{\exp(-\gamma_\mu x) + \Gamma_L \exp(\gamma_\mu x - 2\gamma_\mu L)\} \quad (3)$$

where V_0 is the forward microwave voltage in the source transmission line, Γ_S and Γ_L are the modulator (internal) reflection coefficients at the source ($x=0$) and load ($x=L$) ports, respectively, T is the amplitude transmission coefficient at the source port, ω is the microwave frequency, and $\gamma_\mu = \alpha_\mu + i\beta_\mu$, where α_μ is the microwave attenuation and $\beta_\mu = \omega/v_\mu$, is the wavenumber associated with the microwave phase velocity v_μ.

As an optical wave packet begins to propagate from the modulator input facet at time t_0 and at group velocity v_o, it arrives at position x inside the modulator at time $t = t_0 + x/v_o$, which implies $V_{\rm ac}(x) = V_{\rm ac}(x, t = t_0 + x/v_o)$. For an ideal EAM ($\alpha_\mu = 0, v_\mu = v_o, \Gamma_L = \Gamma_S = 0, T = 1$), $V_{\rm ac}(x) \equiv V_0 \exp(i\omega t_0)$. Normalizing the RF link gain for the general case with respect to the ideal case, we obtain

$$G_{\rm NORM} = \left| \frac{T}{1-\Gamma_L\Gamma_S \exp(-2\gamma_\mu L)} \left\{ \frac{\exp\{(j\beta_o - \gamma_\mu)L\} - 1}{(j\beta_o - \gamma_\mu)L} + \Gamma_L \exp(-2\gamma_\mu L) \frac{\exp\{(j\beta_o + \gamma_\mu)L\} - 1}{(j\beta_o + \gamma_\mu)L} \right\} \right|^2 \quad (4)$$

where $\beta_o = \omega/v_o$. Equation (4) is the normalized TW-EAM frequency response, including effects of impedance mismatch, velocity mismatch, and microwave attenuation. This equation is used in the analysis in the following sections. The microwave reflection coefficients can be calculated from $\Gamma_S = (Z_S - Z_m)/(Z_S + Z_m)$, $\Gamma_L = (Z_L - Z_m)/(Z_L + Z_m)$, and $T = 1 - \Gamma_S$, with Z_S, Z_m, and Z_L defined as the characteristic microwave impedance of the source transmission line, the modulator and the terminator, respectively.

For a short, lumped element device, the terminator port is open, i.e., $\Gamma_L = 1$. If we ignore the microwave attenuation and use the small L approximation in (4), we get,

$$G_{\rm NORM} = \left| \frac{2T}{\exp(j\beta_\mu L) - \Gamma_S \exp(-j\beta_\mu L)} \right|^2 = \left| \frac{2(1-\Gamma_S)}{1-\Gamma_S + (1+\Gamma_S) j\beta_\mu L} \right|^2. \quad (5)$$

Noting that $(1+\Gamma_S)/(1-\Gamma_S) = Z_S/Z_m$, $Z_m = \sqrt{L_m/C_m}$, $\beta_\mu = \omega\sqrt{L_m/C_m}$, where L_m and C_m are the inductance and capacitance per unit length of the modulator, we can rewrite (5) as

$$G_{\rm NORM} = \left| \frac{2}{1 + j\omega Z_S C_m L} \right|^2. \quad (6)$$

Equation (6) can be regarded as the *RC*-limited gain of a lumped element short waveguide modulator with $C_m L$ representing the total modulator capacitance. The factor of 2 in the numerator of (6) is a result of the voltage doubling occurring at the open modulator termination port.

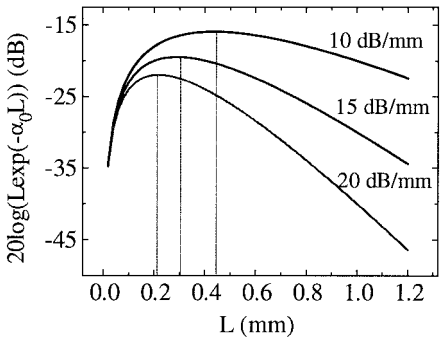

Fig. 1. Optimal modulator length for maximal RF gain with different optical propagation loss.

III. Optical Propagation Loss and Optimal Modulator Length

It is often desirable to lengthen the modulator as much as possible to increase the modulation efficiency. However, there is an upper limit due to the optical propagation loss. Consider the low frequency gain for a TW-EAM. At very low frequency, the modulation voltage $V_{\rm ac}(x)$ for a particular optical wave packet is constant ($=V_0$) along the whole waveguide. The modulated optical power can be expressed as

$$I_{\rm ac} = -I_{\rm in} C^2 \exp(-\alpha_o L - \gamma\alpha_b L)\gamma \frac{d\alpha_b}{dV_b} V_0 L. \quad (7)$$

With a larger L, the optimal dc bias voltage V_b becomes smaller allowing a smaller α_b. For EAM's, the optimal bias point V_b usually results at the normalized transmission ($T = \exp(-\gamma\alpha_b L)$) value of 0.5–0.7. This implies that the term $\exp(-\gamma\alpha_b L)$ in (7) has little dependence on L. The dependence of $d\alpha_b/dV_b$ on L is difficult to model analytically. Usually, $d\alpha_b/dV_b$ is smaller for smaller V_b as L increases. In (7), the most significant terms are L and $\exp(-\alpha_o L)$, the latter denotes the optical propagation loss at zero bias. The optical propagation loss depends on the modulator structural design. For a typical EAM with a 3–4-μm waveguide width and a 0.3–0.4-μm-thick undoped absorption layer, the propagation loss ranges from 15 to 20 dB/mm [1], [10], [12]. Most of the propagation loss comes from the residual absorption at zero bias. For an efficient EAM, the detuning energy between the photon and the absorption layer bandgap cannot be too large. The detuning energy, in turn, directly determines the residual absorption. Hence, in an ultrahigh-speed modulator designed for high-modulation efficiency, the optical propagation loss cannot be reduced much from the above values.

To determine the optimal modulator length L for maximum RF link gain, consider the $L \cdot \exp(-\alpha_o L)$ factor in (7). A plot of $20\log(L\exp(-\alpha_o L))$ versus L is shown in Fig. 1 for different propagation loss. From Fig. 1 it is seen that for an optical propagation loss of 15 dB/mm, the optimal modulator length is 0.3 mm, while that for 20 dB/mm propagation loss is 0.22 mm. Owing to the fact that $d\alpha_b/dV_b$ is smaller for longer L, it will take an optimal length smaller than that predicted in Fig. 1 to maximize the RF link gain. In [13], the optimal modulator length was measured to be 0.17 mm. Since a longer modulator length will not improve either the RF gain or the

TABLE I
MEASUREMENT RESULTS FOR MICROWAVE PROPERTIES OF MODULATOR WAVEGUIDES

Reference	Material	Structure	Device type	w	d_I	n_μ	Attenuation	Z_m
[3]	InAsP/InGaP MQW	Planar-microstrip	Electro-absorption	3 μm	0.9 μm	~3.7	5.6dB/mm @40GHz	30 Ω
[8]	InGaAs/InGaAlAs MQW	Planar-microstrip	Electro -optic	3.9 μm	~0.5 μm	~7	7.3 $dBcm^{-1}GHz^{-1/2}$	25 Ω

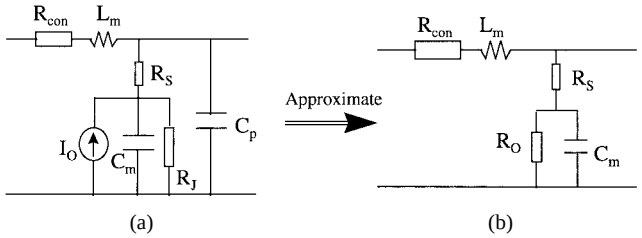

Fig. 2. Quasi-static circuit model for a unit length of TW-EAM transmission line.

bandwidth, modulator lengths exceeding the optimal length predicted in Fig. 1 should be avoided.

IV. MICROWAVE PROPERTIES OF THE TW-EAM WAVEGUIDE

The TW-EAM impedance Z_m, velocity ν_μ and microwave attenuation α_μ can be estimated with a quasi-static circuit model for a unit length of TW-EAM transmission line, as is shown in Fig. 2(a). In this circuit diagram, $R_{\rm con}$ is the conduction resistance, L_m is the inductance, R_S is the device series resistance, C_m is the junction capacitance, R_J is the junction leakage resistance, I_O is the photocurrent governed by electroabsorption, and C_P is the parasitic capacitance. For well-designed EAM's, C_P is typically very small in value and R_J is much larger than the impedance governed by C_m for microwave frequencies beyond 1 GHz. Therefore, both C_P and R_J can be replaced by an electrical open. With these assumptions, the circuit model can be approximated by that shown in Fig. 2(b), where $R_O = (dI_O/dV_J)^{-1}$ is the equivalent ac resistance due to the dependence of the current I_O on the modulator junction voltage V_J. This optical power dependent current path can significantly affect the microwave properties of the TW-EAM at high input optical power.

Using the circuit parameters in Fig. 2(b), all of the relevant microwave properties of a TW-EAM waveguide can be derived from [7]

$$Z_m = \sqrt{(R_{\rm con} + j\omega L_m)\{R_S + R_O/(1 + j\omega R_O C_m)\}} \quad (8)$$

$$\gamma_\mu = \alpha_\mu + j\beta_\mu = \sqrt{(R_{\rm con} + j\omega L_m)/\{R_S + R_O/(1 + j\omega R_O C_m)\}}. \quad (9)$$

The circuit parameters of the TW-EAM waveguide transmission line are generally frequency dependent. However, at frequencies above 1 GHz where all the skin, edge and proximity effects are fully pronounced, L_m, C_m, R_S, and R_O tend to be constants, and $R_{\rm con}$ increases as the square root of frequency. To estimate the circuit parameter values above 1 GHz, experimental results have to be used. Measurements of microwave properties have been reported for waveguides fabricated on InP substrates [3], [8]. Results of this past work are summarized in Table I, where w is the waveguide width, d_I is the intrinsic layer thickness, n_μ is the microwave phase index. n_μ and Z_m are values at 40 GHz for [3] and at 20 GHz for [8].

Since no optical power was used in the above measurements, R_O can be considered as electrical open. Also no measured imaginary part of the impedance was reported. Since the imaginary part is much smaller than the real part at the frequencies considered, the real part can be taken as the measured impedance. Assuming that at 20–40 GHz, $R_{\rm con} \ll \omega L_m$ and $R_S \ll 1/\omega C_m$, (8) and (9) can be greatly simplified. Finally, we obtain

$$Z_m = \sqrt{L_m/C_m}; \qquad \beta_\mu = \omega\sqrt{L_m C_m} \quad (10)$$

$$\alpha_\mu = \frac{R_{\rm con}}{2}\sqrt{C_m/L_m} + \frac{1}{2}R_S\omega^2\sqrt{L_m C_m^3}. \quad (11)$$

From Z_m and β_μ, it can be calculated that for the device in [3], $L_m = 0.37$ nH/mm, $C_m = 0.41$ pF/mm; while for the device in [8], $L_m = 0.58$ nH/mm, $C_m = 0.93$ pF/mm. For 3-μm-wide device in [3], typical $R_S = 1$ Ω·mm; while for 4-μm-wide device in [8], typical $R_S = 0.75$ Ω·mm. Therefore, $R_{\rm con} = 3.5\ \Omega\cdot{\rm mm}^{-1}\cdot{\rm GHz}^{-1/2}$ for [3] and $R_{\rm con} = 2.5\ \Omega\cdot{\rm mm}^{-1}\cdot{\rm GHz}^{-1/2}$ for [8] can be derived.

Consider a standard InGaAsP–InP EAM with a ~3-μm-wide waveguide and a ~0.3-μm-thick intrinsic absorption region. To first-order approximation, taking $R_{\rm con} \propto w^{-1}$ and $C_m \propto w/d_I$, we can infer that $C_m \sim 1.2$ pF/mm [9] and $R_{\rm con} \sim 3.5\ \Omega\cdot{\rm mm}^{-1}\cdot{\rm GHz}^{-1/2}$ for the standard EAM structure. However, L_m may depend on various electrode and waveguide layer parameters. For the standard EAM, L_m can vary significantly but will fall somewhere into the wide inductance range of 0.1–1 nH/mm. The effect of inductance on TW-EAM bandwidth will be numerically investigated in Section VI.

The electroabsorption related resistance R_O is optical power dependent. At low optical power, R_O is simply an open circuit; at high optical power, R_O becomes smaller in value. For example, at 5-dBm input optical power, dI_O/dV_J can be ~0.45 mA/V for a 180-μm-long waveguide [10] implying an R_O of 400 Ω·mm. At higher optical power and/or with a more efficient modulator, dI_O/dV_J can be as large as ~10 mA/V for a 135-μm-long waveguide [11] implying an R_O value of 13.5 Ω·mm.

Substituting $L_m = 0.5$ nH/mm, $C_m = 1.2$ pF/mm, $R_{\rm con} = 3.5\ \Omega\cdot{\rm mm}^{-1}\cdot{\rm GHz}^{-1/2}$, $R_S = 1$ Ω·mm, $R_O = 10^6$ and 20 Ω·mm into (8) and (9), frequency dependent microwave properties for the standard EAM waveguide can be obtained. The calculation results are shown in Fig. 3. Without optical

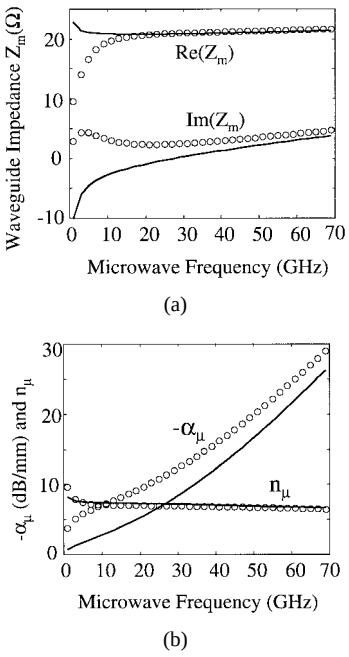

Fig. 3. Frequency dependent microwave properties for a standard EAM waveguide. Solid lines: no optical power, $R_O = 10^6\ \Omega$·mm; symbol lines: high optical power, $R_O = 20\ \Omega$·mm.

power, the curves are very similar to published measurement results. However, at high optical power where R_O drops to small values such as 20 Ω·mm, microwave properties are affected, especially at low frequency. The effect of high optical power on modulator bandwidth will be numerically investigated in Section VI.

Due to the microwave voltage drop across R_S, the normalized link gain has to be modified as

$$LG_{\mathrm{NORM}} = G_{\mathrm{NORM}} \frac{R_O^2}{\left|R_O + (1 + j\omega C_m R_O) R_S\right|^2} \tag{12}$$

with G_{NORM} given by (4).

V. TW-EAM Transit Time Effects

It has been shown that the carrier transit time in the device intrinsic layer is the ultimate limit to the bandwidth of p-i-n photodetectors (PD's) [14]. Since EAM's and PD's are similar in structure, they will share some common carrier transport properties [15]. However, EAM's are principally voltage-controlled devices, while PD's are current–output devices. Consequently, the carrier transit time limit for EAM's and PD's may be different. To ensure the resulting TW-EAM can work at ultrahigh speed, transit time effects on EAM's should be examined.

Fig. 2(b) shows that, under normal operation, the junction ac current in a TW-EAM is mainly composed of two parts. One is the displacement current related to the junction capacitance C_m, another is the ac photocurrent governed by optical absorption. They both come from the external modulation source. When the microwave frequency is close to or beyond the transit time limit, the ac photocurrent will roll off, while the displacement current will not be affected. When the microwave frequency is high enough, $1/\omega C_m \ll R_O$, the displacement current will be much larger than the ac photocurrent. This implies that the transit time limit has little impact on the waveguide microwave properties, although the microwave loss could be slightly reduced due to smaller ac photocurrent.

In PD's, ac photocurrent is the only source of both displacement current and output signal, so that the PD's bandwidth is subject to the transit time limit. However, in EAM's, the ac photocurrent does not critically affect device operation as long as the optical absorption is not affected. For microwave frequencies beyond the transit time limit, the carriers generated by photoabsorption cannot be swept out of the junction promptly. At low optical power, there are few carriers generated, thus the absorption coefficient is not affected by the transit time limit. At high optical power, high-density carriers are generated and accumulate in the junction area at all modulation levels. These accumulated carriers will screen both the biasing and the modulation electrical field and cause dc and ac saturation, which can reduce the modulation efficiency. However, the screening effect will not be severely affected by the modulation voltage, since the accumulated carriers are mainly generated by dc absorption due to the fact that the modulation voltage is generally much smaller than the dc bias voltage.

Consequently, according to the above discussion, carrier transit time effects in EAM's may not significantly deteriorate the modulator performance, including the device bandwidth.

VI. TW-EAM Approaches

From Fig. 3 it is seen that for a typical EAM waveguide, all microwave properties are frequency dependent, microwave attenuation is pretty large, waveguide impedance is far from 50 Ω and has an imaginary part, and the microwave phase index ranges from 10 to 6. There are currently no published reports regarding the optical group index in InP–InGaAsP waveguides. However, the optical group index in a GaAs–AlGaAs waveguide has been measured to be $\sim$3.73 [6], which is larger than the optical phase index of 3.38. For a typical InP–InGaAsP waveguide, whose optical phase index is 3.2–3.3, an optical group index of 3.5 is assumed. This implies a large velocity mismatch for standard 1.3- or 1.55-μm EAM's. Consequently, it seems difficult to achieve a large bandwidth for a TW-EAM with a conventional EAM waveguide with a typical electrode design. In the following, several possible approaches for achieving an ultrahigh-speed TW-EAM will be described.

A. Low-Impedance Matching

A simple way to achieve large TW-EAM bandwidth is to use standard EAM waveguide matching with a low-impedance terminator. This is similar to using a small shunt resistance in L-EAM for broadening the bandwidth. The L-EAM frequency response can be calculated by

$$LG_{\mathrm{NORM}} = \left| \frac{2r}{1 + j\omega C_m L (R_S/L + Z_S r)} \right|^2 \tag{13}$$

where $r = R_{sh}/(R_{sh} + Z_S)$, and R_{sh} is the shunt resistance. Low optical power is assumed.

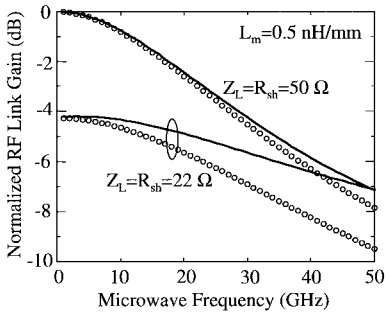

Fig. 4. Effect of low-impedance terminator for TW-EAM (solid lines) and L-EAM (symbol lines).

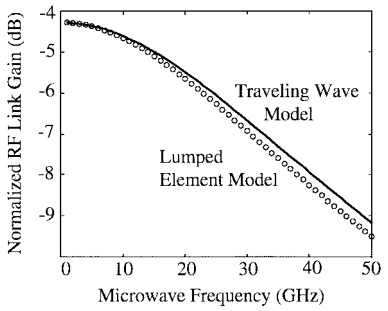

Fig. 5. Validity of (13) for L-EAM checked by TW model.

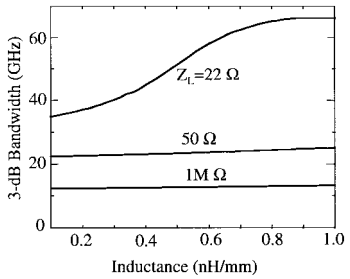

Fig. 6. TW-EAM bandwidth versus waveguide inductance with different terminators.

To compare the performance of a TW-EAM and an L-EAM, the same 0.2-mm-long standard EAM waveguide is assumed in both cases. This implies that they possess the same optical and microwave properties. Also assume $R_{sh} = Z_L$ to ensure a fair comparison. For the standard EAM waveguide, it is shown in Section IV that $L_m = 0.1$ to 1 nH/mm, $C_m = 1.2$ pF/mm, $R_{\rm con} = 3.5\ \Omega{\cdot}{\rm mm}^{-1}{\cdot}{\rm GHz}^{-1/2}$, $R_S = 1\ \Omega{\cdot}$mm, $R_O = 10^6\ \Omega{\cdot}$mm, $L = 0.2$ mm, and $Z_S = 50\ \Omega$. To calculate the frequency response for the resulting TW-EAM, first use (8) and (9) to obtain Z_m, α_μ, and β_μ, then calculate the frequency dependent Γ_S, Γ_L, and T. The above results are substituted into (4) and (12) to calculate the normalized link gain. The frequency response for the L-EAM can be simply calculated using (13). The respective calculated modulator frequency responses are compared in Fig. 4. It is found that with $R_{sh} = Z_L = 50\ \Omega$, the frequency responses are very close for both modulators. They both have approximately 22-GHz bandwidth. However, in Fig. 4, when R_{sh} and Z_L are reduced to 22 Ω, the TW-EAM has significantly better performance than the L-EAM. In this case, the TW-EAM has a bandwidth of about 50 GHz, whereas the L-EAM has only 30-GHz bandwidth. About 4.2-dB low-frequency gain has been sacrificed in both cases as the penalty for broader bandwidth.

In the above calculation for the L-EAM using (13), effects of inductance and conduction resistance are ignored. This may cause inaccuracy. The TW model can be used to check the validity of (13). In the 200-μm-long L-EAM, both 50-Ω RF source transmission line and 22-Ω shunt resistance are connected at the middle point of the waveguide. It is equivalent to two 100-μm-long TW-EAM in parallel, with each TW-EAM source port connected with 100-Ω RF source transmission line and 44-Ω shunt resistance, and the terminator port left open. In this case, T and Γ_S in (4) should be carefully evaluated ($T \neq 1 - \Gamma_S$). The calculation results are plotted in Fig. 5, which shows that the inaccuracy of bandwidth from (13) is only 1 GHz.

To make a 50-GHz bandwidth L-EAM, a 63-μm-long active waveguide was used in [1]. Since a 63-μm-long waveguide is difficult to handle, a selectively regrown passive waveguide section was integrated. Compared with the 200-μm-long standard L-EAM, this 50-GHz L-EAM has sacrificed $\sim$10 dB RF gain, which is $\sim$6 dB larger loss than that of the TW-EAM device in Fig. 4. Furthermore, the optical saturation power for a 200-μm-long TW-EAM should be much larger than the 63-μm-long L-EAM, since the optical absorption is more distributed.

At 50 GHz, with $n_\mu = 7$, the microwave wavelength is $\sim$800 μm. The 200-μm waveguide length is one quarter of the wavelength, which means the microwave voltage is very different along the whole waveguide. This is enough to make the TW effect significant.

In Fig. 6, the effect of waveguide inductance on TW-EAM bandwidth is investigated. When $Z_L > 50\ \Omega$, the waveguide inductance has little impact on TW-EAM bandwidth. However, when $Z_L = 22\ \Omega$, in the L_m range of 0.1–1.0 nH/mm, larger L_m will yield larger bandwidth, and the TW-EAM bandwidth is always larger than the bandwidth of the L-EAM.

Photocurrent generation is inherent in EAM devices. It was shown in Section IV that this current path could significantly alter the waveguide microwave properties at high input optical power. Fig. 7 shows that when high optical power causes R_O to drop to 20 $\Omega{\cdot}$mm, the TW-EAM low-frequency gain drops 1.5 dB, but the bandwidth increases from 50 to 67 GHz. This is because at lower frequency, $1/\omega C_m$ is large compared with R_O, so that the ac photocurrent through R_O is larger causing larger microwave loss. This flattens the TW-EAM frequency response and increases the bandwidth. Even though R_O is not constant throughout the waveguide due to the fact that the absorbed optical power decays exponentially along the waveguide, it can be expected that the TW-EAM bandwidth will not be reduced by the large photocurrent.

B. Reducing Modulator Capacitance

Another approach for implementing a TW-EAM is to make the modulator capacitance per unit length C_m smaller. This increases the modulator impedance and the microwave phase velocity, and both the microwave phase index and the atten-

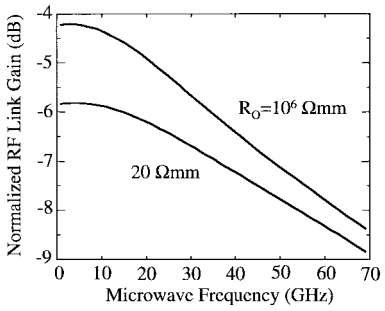

Fig. 7. Effects of high optical power on TW-EAM performance.

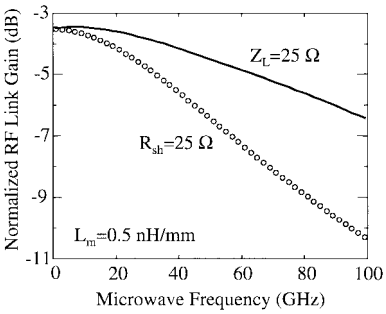

Fig. 8. Frequency response for a TW-EAM with 3-μm waveguide width and 0.5-μm intrinsic region thickness. Symbol line is for L-EAM.

uation loss are reduced. Therefore, by making C_m smaller, all the critical design issues relevant to the TW-EAM can be relieved. However, it is difficult to reduce C_m without sacrificing the RF link gain. To reduce C_m, one has to either increase the intrinsic layer thickness, which will make the modulation voltage less efficient (as $d\alpha_b/dV_b$ becomes smaller), or reduce the waveguide width, which increases the microwave conduction loss and perhaps adds optical coupling loss between the EAM and the fiber pigtails. Although the modulation efficiency will be sacrificed, this approach could extend the TW-EAM bandwidth to 100 GHz.

Consider a 0.2-mm-long InGaAsP–InP TW-EAM with ~3-μm-wide waveguide and ~0.5-μm-thick intrinsic absorption region. With this structure the modulation efficiency will not be significantly sacrificed, and C_m will decrease to ~0.72 pF/mm according to Section IV. Using $L_m = 0.5$ nH/mm, $C_m = 0.72$ pF/mm, $R_{\rm con} = 3.5\ \Omega{\cdot}{\rm mm}^{-1}\ {\rm GHz}^{-1/2}$, $R_S = 1\ \Omega{\cdot}$mm, and $R_O = 10^6\ \Omega{\cdot}$mm, the calculated modulator frequency response is plotted in Fig. 8. It is seen that the TW-EAM bandwidth is 100 GHz with $Z_L = 25\ \Omega$, whereas the L-EAM with the same structure and $R_{sh} = 25\ \Omega$ only has 45-GHz bandwidth. If L_m is larger than 0.5 nH/mm, the TW-EAM bandwidth can be extended beyond 100 GHz.

C. Distributing Modulation Region

A third approach to realizing the TW-EAM involves distributing the modulation region. It is possible to use separate RF transmission lines to feed the microwave signal discretely to modulate the optical waveguide. In this case, the design for the microwave transmission line is decoupled from the design of the optical waveguide. A similar approach has been investigated for a velocity-matched distributed photodetector

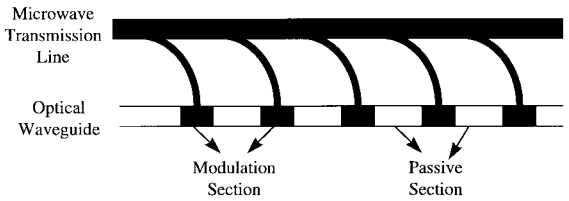

Fig. 9. Schematic diagram of modulation distributed TW-EAM.

[16] and an electrooptic modulator [17]. Fig. 9 illustrates the concept for a TW-EAM with modulation region periodically distributed. Generally, to ensure that the optical waveguide capacitance is negligible compared to that of the microwave transmission line, the modulation sections should be much shorter than the passive sections in the optical waveguide. Using this approach, the microwave transmission line can be separately and independently designed to achieve very small microwave attenuation. Excellent impedance matching with 50 Ω and excellent velocity matching with an optical waveguide can be possible for ultra large modulation bandwidth operation. However, special care must be given to the optical waveguide design, as is discussed in the following.

If the optical confinement factor γ for the absorption layer in the modulation section is made very small, efficient modulation might require a very long optical waveguide since the optical absorption coefficient is not very large for a well-designed EAM. This very long optical waveguide can result in large optical propagation loss. However, if a large γ is used with a structure that uses the same optical waveguide in both the modulation and passive sections, the passive sections will contribute significantly to the optical propagation loss. A different optical waveguide geometry for modulation and passive sections can be designed so that γ is large in the modulation sections, and no significant residual absorption occurs in the passive sections. For this approach, care must be given to minimize the accumulating mode coupling loss between the different sections in order to realize an efficient TW-EAM.

VII. Summary

From the analysis presented in this paper, a high-efficiency ultralarge-bandwidth TW-EAM is feasible. The TW-EAM can have similar low-frequency RF link gain as the L-EAM while maintaining a large modulation bandwidth. Photocurrent generation at high optical power can slightly improve the TW-EAM bandwidth although it has the effect of lowering the RF link gain. Additionally, carrier transit time effects do not limit the bandwidth of a TW-EAM as is the case with a p-i-n PD. Due to the optical propagation loss, the optimal modulator length is found to be 0.2–0.3 mm. A longer modulator length is not suitable in view of both bandwidth and RF gain considerations. Based on this, three TW-EAM approaches have been examined. The low-impedance matching approach is the easiest one, and can extend the electrical bandwidth to above 50 GHz. Optimizing the waveguide structure and reducing its capacitance per unit length, bandwidths beyond 100 GHz are achievable at the expense of sacrificing some RF link gain. Distributing the modulation region and using

a discrete transmission line could lead to an even larger modulator bandwidth, but the optical waveguide design needs further investigation.

REFERENCES

[1] T. Ido, S. Tanaka, M. Suzuki, M. Koizumi, H. Sano, and H. Inoue, "Ultra-high-speed multiple-quantum-well electro-absorption modulators with integrated waveguides," *J. Lightwave Technol.*, vol. 14, pp. 2026–2034, 1996.

[2] K. Kawano, M. Kohtoku, M. Ueki, T. Ito, S. Kondoh, Y. Noguchi, and Y. Hasumi, "Polarization-insensitive travelling-wave electrode electroabsorption (TW-EA) modulator with bandwidth over 50 GHz and driving voltage less than 2 V," *Electron. Lett.*, vol. 33, pp. 1580–1581, 1997.

[3] H. H. Liao, X. B. Mei, K. K. Loi, C. W. Tu, P. M. Asbeck, and W. S. C. Chang, "Microwave structures for traveling-wave MQW electroabsorption modulators for wide band 1.3 μm photonic links," in *Proc. SPIE, Optoelectronic Integrated Circuits*, 1997, vol. 3006, pp. 291–300.

[4] S. Z. Zhang, Y. J. Chiu, P. Abraham, and J. E. Bowers, "25-GHz polarization-insensitive electroabsorption modulators with traveling-wave electrodes," *IEEE Photon. Technol. Lett.*, vol. 11, pp. 191–193, 1999.

[5] W. W. Rigrod and I. P. Kaminow, "Wide-band microwave light modulation," *Proc. IEEE*, vol. 51, pp. 137–140, 1963.

[6] R. Spickermann, S. R. Sakamoto, and N. Dagli, "GaAs–AlGaAs traveling wave electro-optic modulators," in *Proc. SPIE, Optoelectronic Integrated Circuits*, 1997, vol. 3006, pp. 272–279.

[7] D. M. Pozar, *Microwave Engineering.* Reading, MA: Addison-Wesley, 1990, pp. 94–97.

[8] M. M. Mihailidi, J. E. Zucker, M. D. Feuer, M. N. Khan, T. Y. Chang, and N. J. Sauer, "Microwave properties of traveling-wave InGaAs/InGaAlAs quantum-well optical waveguide modulators," *Microwave Opt. Technol. Lett.*, vol. 10, pp. 204–207, 1995.

[9] K. K. Loi, X. B. Mei, J. H. Hodiak, C. W. Tu, and W. S. C. Chang, "38 GHz bandwidth 1.3 μm MQW electroabsorption modulators for RF photonic links," *Electron. Lett.*, vol. 34, pp. 1018–1019, 1998.

[10] G. L. Li, R. B. Welstand, W. X. Chen, J. T. Zhu, S. A. Pappert, C. K. Sun, Y. Z. Liu, and P. K. L. Yu, "Novel bias control of electroabsorption waveguide modulator," *IEEE Photon. Technol. Lett.*, vol. 10, pp. 672–674, 1998.

[11] R. B. Welstand, S. A. Pappert, D. T. Nichols, L. J. Lembo, Y. Z. Liu, and P. K. L. Yu, "Enhancement in electroabsorption waveguide modulator slope efficiency at high optical power," *IEEE Photon. Technol. Lett.*, vol. 10, pp. 961–963, 1998.

[12] K. Yamada, H. Murai, I. Nakamura, Y. Matsui, and I. Ogawa, "Low polarization dependence ($<$0.3 dB) in an EA modulator using a polyimide-buried high-mesa ridge structure with an InGaAsP bulk absorption layer," *Electron. Lett.*, vol. 31, pp. 237–238, 1995.

[13] K. K. Loi, X. B. Mei, J. H. Hondiak, K. N. Cheng, L. Shen, H. H. Wieder, C. W. Tu, and W. S. C. Chang, "Experimental study of efficiency-bandwidth tradeoff of electroabsorption waveguide modulators for microwave photonic links," in *Proc. IEEE LEOS*, 1997, vol. 1, pp. 142–143.

[14] W. W. Gartner, "Depletion-layer photoeffects in semiconductors," *Phys. Rev.*, vol. 116, pp. 84–87, 1959.

[15] T. Ido, H. Sano, S. Tanaka, and H. Inoue, "Frequency-domain measurement of carrier escape times in MQW electro-absorption optical modulators," *IEEE Photon. Technol. Lett.*, vol. 7, pp. 1421–1423, 1995.

[16] L. Y. Lin, M. C. Wu, T. Itoh, T. A. Vang, R. E. Muller, D. L. Sivco, and A. Y. Cho, "Velocity-matched distributed photodetectors with high-saturation power and large bandwidth," *IEEE Photon. Technol. Lett.*, vol. 8, pp. 1376–1378, 1996.

[17] R. G. Walker, "High-speed III–V semiconductor intensity modulators," *IEEE J. Quantum Electron.*, vol. 27, pp. 654–667, 1991.

G. L. Li (S'97), photograph and biography not available at the time of publication.

C. K. Sun, photograph and biography not available at the time of publication.

S. A. Pappert, photograph and biography not available at the time of publication.

W. X. Chen, photograph and biography not available at the time of publication.

P. K. L. Yu (S'79–M'84–SM'90), photograph and biography not available at the time of publication.